THE JOURNAL OF PHYSICAL CHEMISTRY B

Article

pubs.acs.org/JPCB

Supramolecular Polymer Transformation: A Kinetic Study

Jonathan Baram, Haim Weissman, and Boris Rybtchinski*

Department of Organic Chemistry, The Weizmann Institute of Science, Rehovot 76100, Israel

Supporting Information

ABSTRACT: Investigation of supramolecular kinetics is essential for elucidating self-assembly mechanisms. Recently, we reported on a noncovalent system involving a bolaamphiphilic perylene diimide dimer that is kinetically trapped in water but can rearrange into a different, more ordered assembly in water/THF mixtures (*Angew. Chem. Int. Ed.* **2014**, *53*, 4123). Here we present a kinetic mechanistic study of this process by employing UV−vis spectroscopy. The transformation exhibits a rapid decrease in the red-shifted absorption band, which is monitored in order to track the kinetics at different temperatures (15−50 °C) and concentrations. Fitting the data with the 1D KJMA (Kolmogorov−Johnson−Mehl−Avrami) model affords the activation parameters. The latter as well as seeding experiments indicates that the transformation occurs without the detachment of covalent units, and that hydration dynamics plays a significant role in nucleation, with entropic factors being dominant. Switching off the transformation, and the formation of off-pathway intermediates were observed upon heating to temperatures above 55 °C. These insights into kinetically controlled supramolecular polymer transformations provide mechanistic information that is needed for a fundamental understanding of noncovalent processes, and the rational design of noncovalent materials.

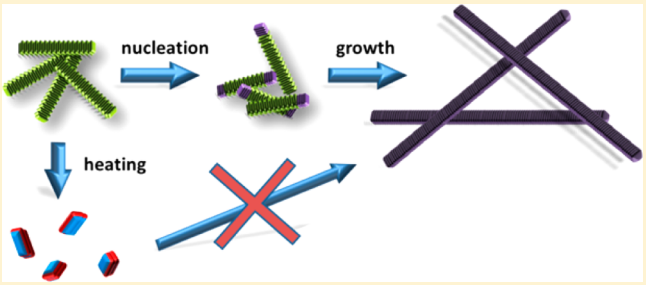

INTRODUCTION

Supramolecular polymers are one-dimensional assemblies that are formed by dynamic noncovalent intermolecular interactions.[1,2] Supramolecular polymerization processes that are under thermodynamic control are well-known and have been extensively studied.[3] However, a variety of noncovalent self-assembly processes, including supramolecular polymerization, can proceed under kinetic control,[4−6] enabling kinetic mechanistic studies.[7−10] Elucidating the underlying mechanisms in noncovalent self-assembly is critical for the rational design of functional organic materials, where kinetically controlled assembly is common, but not well understood. Importantly, in biological polymerization systems, such as actin and microtubules, mechanistic kinetic studies were critical in elucidating the key parameters of the assembly dynamics.[11−13]

Very recent thermodynamic studies on supramolecular polymerization have continued to uncover the complex nature of these processes, which can proceed by cooperative, isodesmic, or other mechansims.[14−18] Kinetic studies on noncovalent polymerization are rare, although they are recognized as the key to unraveling supramolecular transformation mechanisms.[4,19] Recent in-depth kinetic studies on supramolecular polymerization revealed a complex process leading to polymer formation that is governed by a nucleation/growth-type mechanism, and which includes several competing supramolecular polymerization pathways.[7,10,20] Underscoring the complexity of kinetically controlled noncovalent transformations, our kinetic/structural study on crystalline self-assembly in aqueous media revealed the importance of prenucleation states and desolvation energetics.[8]

We have recently shown that strong hydrophobic interactions result in stable noncovalent polymer isomers that are based on a single covalent unit.[21] These isomers have different structures and electronic/photonic properties, and are stable in water, even upon prolonged heating to 100 °C. The covalent unit employed in this system, a poly(ethylene glycol) (PEG) functionalized perylene diimide (PDI) dimer (compound **1**), forms short fibers when dissolved in water or in water/THF mixtures. This form was designated as "**1G**" (Figure 1). Although indefinitely stable in water, in water/THF mixtures **1G** slowly rearranges into long fibers, accompanied by a color change from green to brown-purple.[21] The purple fiber assembly is designated as **1P** (Figure 1). The difference in the photonic and electronic properties of **1P** and **1G** are due to different interactions between the aromatic cores.

Herein, we report on a kinetic mechanistic study of **1G** → **1P** transformation. This process follows a nucleation/growth mechanism, revealing the critical role of prenucleation assemblies, and allowing the observation of off-pathway intermediates. Extremely sharp nucleation-to-growth transition and convenient temperature regulation of off-pathway switching allow a high degree of control over the noncovalent polymerization.

Received: August 6, 2014
Revised: September 17, 2014
Published: September 19, 2014

dx.doi.org/10.1021/jp507945t | *J. Phys. Chem. B* 2014, 118, 12068−12073

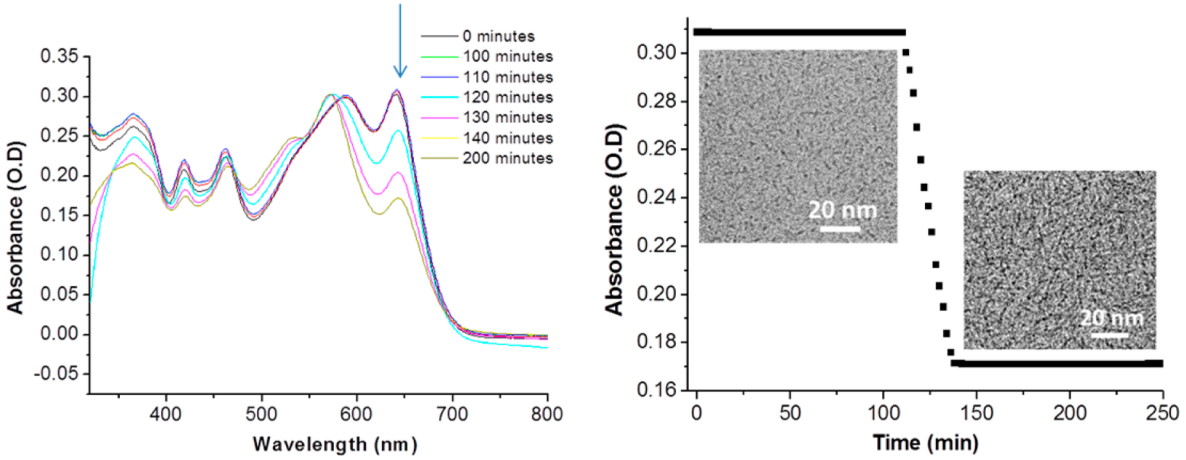

Figure 1. Left: time-dependent UV−vis spectra of compound **1** in a water:THF mixture (6:4; v/v; 20 °C; 4×10^{-5} M). Right: time-dependent intensity change at 640 nm. Insets: cryo-TEM images of **1G** (top, after 2 min of evolution) and **1P** (bottom, fully evolved) in a water:THF mixture (6:4; v/v).

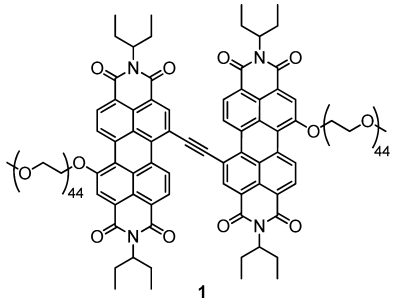

1

Table 1. Measured lengths and Widths (from Cryo-TEM Images) of 1G Fibers, 10^{-4} M in Water:THF (60:40; v/v) at Different Temperatures, up to 2.5 min after Preparation

temperature (°C)	fiber length (nm)	fiber width (nm)
20	19 ± 4	2.1 ± 0.3
30	21 ± 8	2.2 ± 0.2
40	19 ± 8	2.1 ± 0.2
50	23 ± 7	2.1 ± 0.2

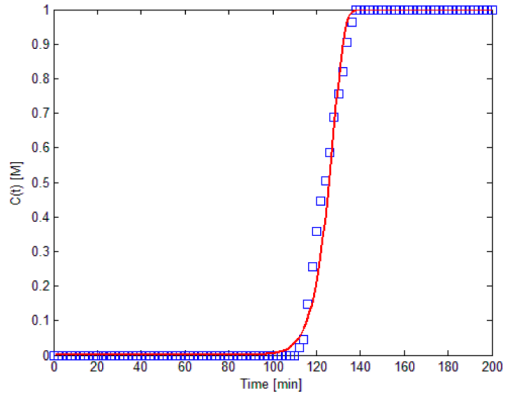

Figure 2. Kinetic KJMA fit (red line) of the experimental kinetics (blue squares) at 20 °C (4×10^{-5} M).

RESULTS AND DISCUSSION

Kinetic Studies. 1G → 1P transformation takes place with 10−40% (volume ratio) THF content in aqueous solutions, the transformation being faster at higher THF content, as observed by UV−vis. This is consistent with our previous observations that organic solvent leads to enhanced dynamics via lowering the kinetic barriers arising from hydrophobic interactions.[8,22] THF content above 50% leads to disaggregation. **1G → 1P** transformation kinetics was studied in water:THF=6:4 (v/v) solutions. The assembly process was monitored using UV−vis spectroscopy at five different temperatures (15, 20, 30, 40, and 50 °C).

In order to induce aggregation, a solution of **1** in THF (molecularly disaggregated, as evidenced by the UV−vis spectrum) was injected into water to yield a green solution of **1** in water:THF = 60:40 (v/v). This fast aggregation results in the formation of short fibers (**1G**, 19 ± 4 nm in length, 2.1 ± 0.3 nm in width, Figures 1 and S1(Supporting Information)) similar to the ones we observed in pure water.[21] **1G** undergoes a transformation (within hours or minutes, depending on the conditions) into long nanofibers (**1P**, 1.7 ± 0.3 nm in width, and more than 150 nm in length, Figures 1 and S1), accompanied by a color change from green to purple-brown. The kinetics of this process was monitored utilizing the decrease in the intensity of the PDI absorption band at 640 nm, characteristic of the **1G → 1P** transformation (Figure 1). This UV−vis spectral change is due to the *J*-aggregate character (slipped stack, leading to red-shifted absorption) of **1G**, which, upon transforming into **1P**, having a *H*-aggregate structure,[21] results in a decrease in the 640 nm peak intensity.

The kinetic trace for the **1G → 1P** transformation was obtained by plotting the intensity of the 640 nm peak over time. The resulting sigmoid-shaped graph (Figure 1) exhibits kinetic behavior typical of nucleation/growth autocatalytic processes, revealing a relatively long lag time (nucleation), followed by a sharp decrease in the intensity of absorption, eventually reaching a plateau (growth). This process is characterized by a remarkably sharp nucleation-to-growth transition and high growth rates in comparison with those of the nucleation process.

In order to further probe the nucleation−growth mechanism, we examined the effect of seeding. A seed solution (fully evolved **1P**, 10 mol %) was added to **1G** at various stages of self-assembly. The mixing of the seeds with **1G** during the lag time did not result in significant changes in the nucleation times relative to the nonseeded systems, the same being true for the growth process. This indicates that the **1P** seeds do not interact

dx.doi.org/10.1021/jp507945t | J. Phys. Chem. B 2014, 118, 12068−12073

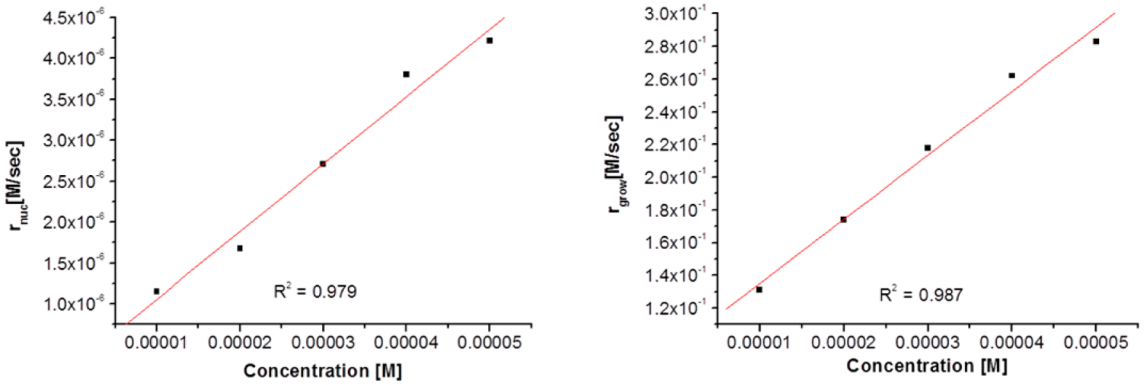

Figure 3. Concentration dependence of the nucleation (A) and growth (B) reaction rates.

Table 2. Nucleation and Growth Reaction Rate Constants at Different Temperatures

T (°C)	k_{nuc} (s^{-1})	k_{grow} (s^{-1})
15	0.057	3390
20	0.082	3920
30	0.144	8430
40	0.152	14 300
50	0.177	24 050

efficiently with **1G**. Apparently, strong hydrophobic interactions in **1G** hinder the dissociation of individual molecules and their binding to the seed. Interaction between the termini of **1G** and **1P**, which may lead to enhanced nucleation, appears to be ineffective as well. Furthermore, addition of sonicated **1P** seeds (intended to increase the number of termini by breaking **1P** fibers) to **1G** also did not result in significant changes in kinetics (Figure S3). The lack of efficient interactions between the initially formed assembly and the seed has been recently observed by us in the case of crystalline self-assembly.[8] In order to assess the stochastic nature of the nucleation event, we performed independent assembly experiments, in which we compared the observed lag times, in accordance with literature procedures.[23] These experiments revealed that the lag time variability was very low (not exceeding 7%, Table S1). The seeding and stochastic variability experiments underscore the stability of the prenucleation aggregates (**1G**), and their critical role in assembly evolution.

We employed the Kolmogorov, Johnson, Mehl, and Avrami (KJMA) nucleation/growth isothermal transformation model to fit the experimental data in order to extract nucleation and growth rate constants. KJMA models were initially used to elucidate the crystallization kinetics and structural changes in metal alloys,[24,25] and have been used since then to describe the assembly kinetics of lipids,[26] polymers,[27] and even DNA replication processes.[28] We have recently used the 2D KJMA model in a kinetic study of crystalline self-assembly in aqueous medium.[8] The most suitable model for describing the structural evolution in the case of **1G** → **1P** supramolecular polymer transformations is a 1D version of the KJMA model.[25,29]

In the KJMA models the growth rate is considered to be isotropic, but the nucleation rate depends on the reaction's evolution, meaning that the nucleation is faster at the beginning and later it slows down as the material is transformed into its ordered state. According to the KJMA model, the nucleation originates from *germ nuclei*, certain structural heterogeneities that exist in the material before the assembly process starts.[24] This is based on the experimental observations that nucleation is almost entirely initiated from such phase heterogeneities.

In order to fit the kinetics, we converted the data to a concentration fraction of ordered material ζ (eq 1):

$$\zeta = \frac{C(t)}{C_{max}} = \frac{\omega_{(t)} - \omega_0}{\omega_{max} - \omega_0} \quad (1)$$

where $C(t)$ is the concentration of ordered material (**1P**) at time t, C_{max} is the maximal concentration of ordered material (fully evolved **1P**), $\omega_{(t)}$ is the UV−vis signal (at 640 nm) intensity at time t, ω_0 is the UV−vis signal intensity at time 0, and ω_{max} is the UV−vis signal intensity obtained for a fully evolved **1P** at a given concentration.

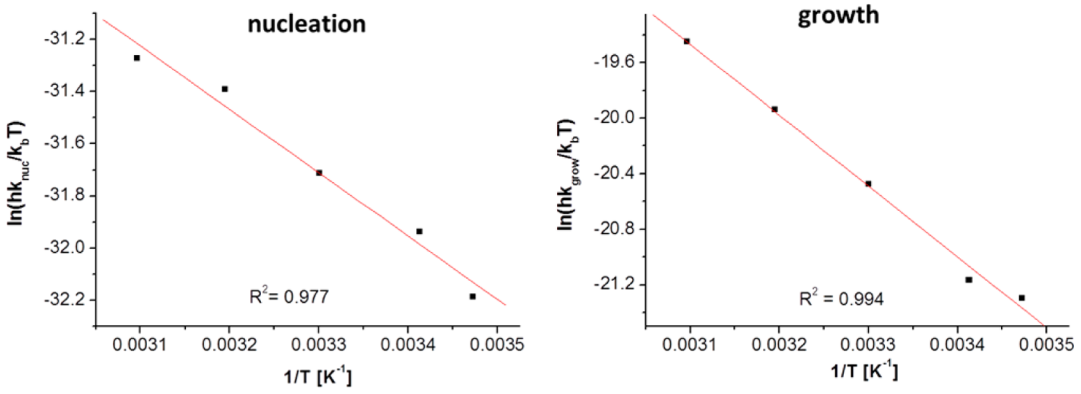

Figure 4. Eyring plots.

dx.doi.org/10.1021/jp507945t | J. Phys. Chem. B 2014, 118, 12068−12073

Table 3. Activation Parameters Extracted from the Eyring Plots

T [K]	$\Delta H^{\neq}$ [kcal/mol]	$\Delta S^{\neq}$ [kcal/(mol K)]	$T\Delta S^{\neq}$ [kcal/mol]	$\Delta G^{\neq}$ [kcal/mol]
		nucleation		
288	4.83 ± 0.42	−0.047 ± 0.0014	−13.54 ± 0.4	18.37 ± 0.83
293	4.83 ± 0.42	−0.047 ± 0.0014	−13.77 ± 0.41	18.6 ± 0.84
303	4.83 ± 0.42	−0.047 ± 0.0014	−14.24 ± 0.42	19.07 ± 0.85
313	4.83 ± 0.42	−0.047 ± 0.0014	−14.71 ± 0.44	19.54 ± 0.86
323	4.83 ± 0.42	−0.047 ± 0.0014	−15.18 ± 0.45	20.01 ± 0.88
		growth		
288	10.14 ± 0.47	−0.0072 ± 0.0016	−2.08 ± 0.44	12.23 ± 0.91
293	10.14 ± 0.47	−0.0072 ± 0.0016	−2.12 ± 0.45	12.26 ± 0.92
303	10.14 ± 0.47	−0.0072 ± 0.0016	−2.19 ± 0.47	12.34 ± 0.94
313	10.14 ± 0.47	−0.0072 ± 0.0016	−2.27 ± 0.48	12.41 ± 0.95
323	10.14 ± 0.47	−0.0072 ± 0.0016	−2.34 ± 0.5	12.48 ± 0.97

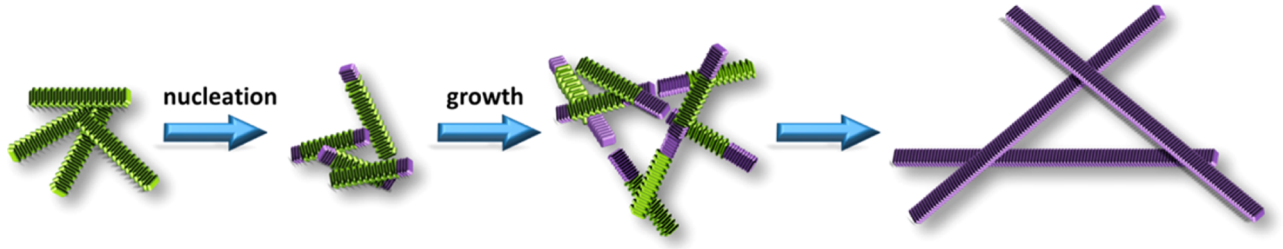

Figure 5. Schematic illustration of the supramolecular polymer transformation.

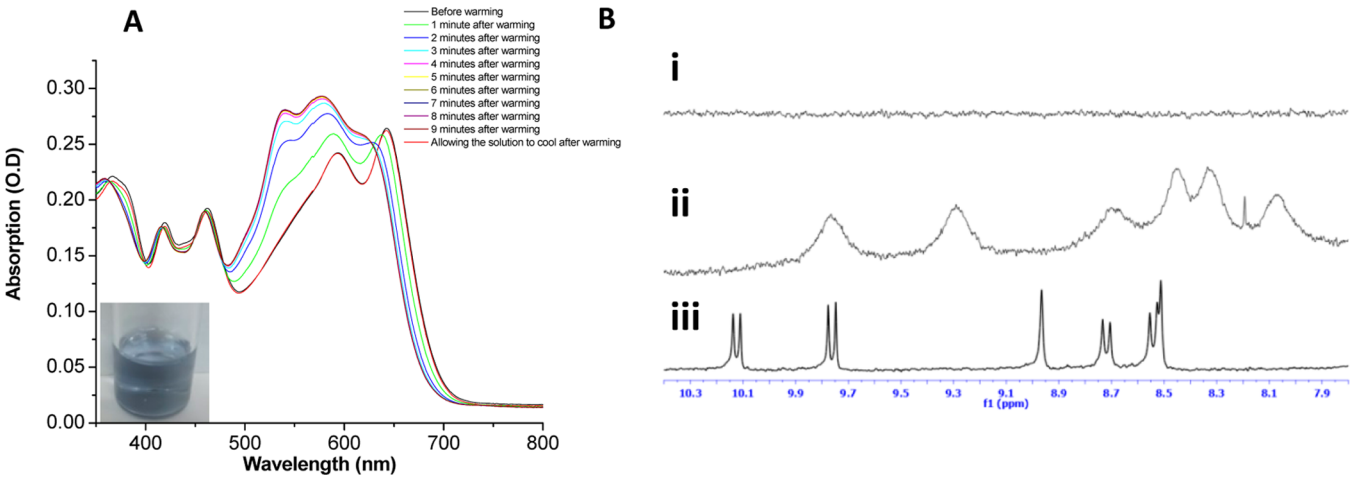

Figure 6. (A) UV−vis spectrum of **1** in water:THF (6:4, v/v) before and after warming to 60 °C (328 K), as well as after allowing the solution to cool to room temperature. Inset: photograph of the warmed solution. (B) Aromatic region of the ^{1}H NMR spectra of **1** (2.0 mM) in (i, ii) D_2O:THF-d_8 (6:4; v/v) at 293 K (i), 328 K (ii), and in $CDCl_3$ at 293 K (iii).

The fraction of the organized material, ζ, in the 1D KJMA model is given by eq 2:[25]

$$\zeta = 1 - \exp\left(\frac{\left(-\frac{\pi}{4}*N_0*\delta^2*\Gamma\right)(e^{\nu} - 1)}{\nu}\right) \quad (2)$$

where N_0 is the density of the nucleation sites (or "germ nuclei", specific sites from which the nucleation starts) per volume of material (nuclei/nm^3), t is the time (s), Γ is the growth velocity (nm/s, the kinematic quantity related to the speed of the fiber growth), δ is the **1G** fiber diameter (10.2 nm), and ν is the probability frequency of the formation of a nucleus per unit time (s^{-1}).

Since the growth is one-dimensional, the most probable germ nucleation sites are the fiber termini, since these differ from the rest of the fiber; they represent structural heterogeneities. The number of germ nuclei per material volume, N_0, was estimated by analyzing the cryo-TEM images. Briefly, N_0 was calculated by assuming two termini for each fiber, and dividing the number of termini by the fiber volume measured immediately after preparing the sample (Table 1). The length of the initially formed fibers does not significantly depend on temperature (Table 1), resulting in an N_0 value of 0.0047 germ nuclei/nm^3, which was used in the KJMA model fits.

Fitting eq 2 to the data (Figures 2 and S2) yields the nucleation *probability frequency* (ν) and the *growth velocity* (Γ). The nucleation rate r_{nuc} is defined as the nucleation rate at time 0 (before any constraints operate on it), and in KJMA model,

dx.doi.org/10.1021/jp507945t | J. Phys. Chem. B 2014, 118, 12068−12073

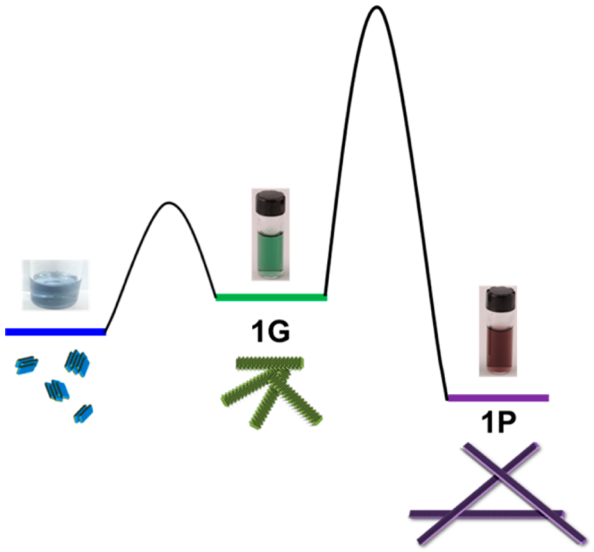

Figure 7. Energy diagram describing the system at 60 °C.

$r_{nuc} = N_0 \times \nu$ (nm^{-3} s^{-1}).[8] The growth rate is obtained from the kinematic velocity Γ (the growth of the 1D crystal front in nm/sec) via scaling by the molecular density, d (in molecules/nm^3), and the molecular size ($L_{molecule}$, the thickness of a molecular unit added to the assembly), $r_{grow} = (\Gamma/L_{molecule}) \times d$ (nm^{-3} s^{-1}). $L_{molecule}$ and d were calculated from the molecular models and were found to be 0.466 nm and 0.35 nm^{-3}, respectively. Both the nucleation and growth processes show linear concentration dependence, thus confirming the first-order kinetics. The rate constants, k_{nuc} and k_{grow}, are derived from the slope of the rate/concentration graphs (Figure 3 and Table 2).

According to Eyring transition state theory, $k = (k_BT/h)\exp(-\Delta G^{\neq}/RT)$, resulting in linear equation $\ln(kh/k_BT) = -(\Delta H^{\neq}/R)\,(1/T) + (\Delta S^{\neq}/R)$. The corresponding Eyring plots are presented in Figure 4, yielding the enthalpy and entropy of activation (Table 3).

The activation parameters for the nucleation process are consistent with the rearrangement at the fiber termini (representing germ nuclei), which involves a change in the hydration pattern, without significant detachment of molecular units. According to this scenario, there is a rearrangement leading to a change in the stacking geometry, resulting in constrained dynamics of the hydration layer.[27] Thus, the negative activation entropy is a major contributor to the activation barrier, suggesting decreased dynamics of the solvation layer upon transformation. Such behavior is consistent with the absence of a significant exposure of hydrophobic surfaces (detachment of the molecular units) to the aqueous medium, which is expected to lead to a larger enthalpic contribution due to unfavorable hydrophobic hydration (breaking multiple hydrogen bonds by a large surface).[30] This hypothesis is also in agreement with the seeding experiments that indicate stability of **1G** toward dissociation. Furthermore, heating above 55 °C, which leads to substantial disaggregation, does not lead to the formation of **1P** (see below), indicating that the **1G** → **1P** transformation proceeds without full detachment of covalent building blocks. Molecular rearrangement itself may also contribute to the entropic barrier. Desolvation, which is characterized by large positive activation enthalpy and entropy,[31,32] is not a major factor contributing to activation barriers, unlike in the case of crystalline self-assembly recently reported by us.[8] The growth process has an entropy of activation that approaches zero and a moderate enthalpy of activation. This process may involve molecular rearrangements, fiber fusion, and slight changes in the hydration dynamics, characterized by a moderate enthalpic activation barrier. Cryo-TEM studies indicate that fibers that are substantially longer than those observed during the nucleation process are formed toward the end of the growth process, confirming that fiber fusion occurs during the growth process rather than during nucleation. The suggested mechanism underlying the **1G** → **1P** transformation is presented in Figure 5.

Off-Pathway Intermediates. Although the rates of nucleation and growth in the **1G** → **1P** transformation increase with rising temperatures (in 15−50 °C range), at higher temperatures an additional process takes place. Heating freshly made water:THF (6:4, v/v) **1G** solutions to 60 °C results in a UV−vis spectrum very different from that of **1P** (Figure 6A), exhibiting a blue-shifted peak with three well-resolved bands, resembling the structure of the absorption peak typical of disaggregated **1**.[18] Remarkably, this spectral change is reversible and the spectrum of **1G** is restored rapidly after the solution is cooled, which can be repeated multiple times. To further investigate the changes induced by heating to high temperatures, we performed temperature-dependent ^{1}H NMR measurements in a D_2O:THF-d_8 = 6:4 solution (Figure 6B). As expected, since at 20−50 °C the assemblies of **1** are highly aggregated, the aromatic region is completely flat, whereas in the aliphatic region only the PEG signal can be clearly identified. However, at 55 °C, both the aliphatic and aromatic signals of the perylene diimide system are clearly seen in the ^{1}H NMR spectrum (Figure 6B). Similar broadened signals and upfield shifts in the ^{1}H NMR spectrum were observed for small PDI-based aggregates (dimers).[33] Thus, significant disaggregation, accompanied by a change in the stacking patterns, occurs upon heating to 55 °C. Notably, if warmed to 55−60 °C, the system remains unchanged for hours, whereas cooling below 50 °C results in rapid formation of **1G**, which subsequently is transformed into **1P**. Figure 7 presents the energy profile of the system at 60 °C: the formation of off-pathway (small) aggregates becomes more facile (kinetically) than the **1G** → **1P** transformation, and the latter is switched off completely since **1G**, which is a critical intermediate, is predominantly converted into smaller aggregates (off-pathway intermediates). Overall, heating to 55−60 °C directs the system off the **1G** → **1P** pathway, and allows controlling the supramolecular process by switching off the **1G** → **1P** transformation. Evidently, **1G** is the on-pathway intermediate required for the formation of **1P**.

■ CONCLUSIONS

A kinetic study of supramolecular fiber reorganization revealed a nucleation/growth process. This noncovalent transformation proceeds without detachment of the covalent units, as indicated by the activation parameters, along with the seeding and temperature-dependent experiments. Upon heating at 55−60 °C, off-pathway intermediates are observed, allowing one to switch off the **1G** → **1P** transformation. Relatively slow nucleation and rapid growth underscore the importance of the initial reorganization process that takes place during the nucleation stage. When such a process occurs, further growth is very facile. Activation parameters imply that the hydration dynamics plays a significant role in nucleation, with entropic factors being dominant. These insights into kinetically

controlled supramolecular polymer transformations provide mechanistic information that is needed for a fundamental understanding of the noncovalent processes, and may assist in the rational design of noncovalent materials.

■ ASSOCIATED CONTENT

Supporting Information

Additional experimental procedures, electron microscopic images, spectroscopic data, and kinetic analysis. This material is available free of charge via the Internet at http://pubs.acs.org

■ AUTHOR INFORMATION

Corresponding Author

*(B.R.) E-mail: boris.rybtchinski@weizmann.ac.il.

Notes

The authors declare no competing financial interest.

■ ACKNOWLEDGMENTS

This work was supported by grants from the Israel Science Foundation, the Minerva Foundation, the Gerhardt M. J. Schmidt Minerva Center of Supramolecular Architecture, and the Helen and Martin Kimmel Center for Molecular Design. The EM studies were conducted at the Irving and Cherna Moskowitz Center for Nano and Bio-Nano Imaging (Weizmann Institute).

■ REFERENCES

(1) Brunsveld, L.; Folmer, B. J. B.; Meijer, E. W.; Sijbesma, R. P. Supramolecular polymers. *Chem. Rev.* **2001**, *101*, 4071−4097.
(2) Aida, T.; Meijer, E. W.; Stupp, S. I. Functional supramolecular polymers. *Science* **2012**, *335*, 813−8177.
(3) de Greef, T. F. A.; Smulders, M. M. J.; Wolffs, M.; Schenning, A. P. H. J.; Sijbesma, R. P.; Meijer, E. W. Supramolecular Polymerization. *Chem. Rev.* **2009**, *109*, 5687−5754.
(4) Korevaar, P. A.; de Greef, T. F. A.; Meijer, E. W. Pathway Complexity in π-Conjugated Materials. *Chem. Mater.* **2014**, *26*, 576−586.
(5) Lohr, A.; Würthner, F. Chiral Amplification, Kinetic Pathways, and Morphogenesis of Helical Nanorods upon Self-assembly of Dipolar Merocyanine Dyes. *Isr. J. Chem.* **2011**, *51*, 1052−1066.
(6) Rybtchinski, B. Adaptive Supramolecular Nanomaterials Based on Strong Noncovalent Interactions. *ACS Nano* **2011**, *5*, 6791−6818.
(7) Korevaar, P. A.; George, S. J.; Markvoort, A. J.; Smulders, M. M. J.; Hilbers, P. A. J.; Schenning, A. P. H. J.; De Greef, T. F. A.; Meijer, E. W. Pathway complexity in supramolecular polymerization. *Nature* **2012**, *481*, 492−496.
(8) Tidhar, Y.; Weissman, H.; Tworowski, D.; Rybtchinski, B. Mechanism of Crystalline Self-Assembly in Aqueous Medium: A Combined Cryo-TEM/Kinetic Study. *Chem.—Eur. J.* **2014**, *20*, 10332−10342.
(9) Zeng, F. W.; Zimmerman, S. C.; Kolotuchin, S. V.; Reichert, D. E. C.; Ma, Y. G. Supramolecular polymer chemistry: design, synthesis, characterization, and kinetics, thermodynamics, and fidelity of formation of self-assembled dendrimers. *Tetrahedron* **2002**, *58*, 825−843.
(10) Ogi, S.; Sugiyasu, K.; Manna, S.; Samitsu, S.; Takeuchi, M. Living supramolecular polymerization realized through a biomimetic approach. *Nat. Chem.* **2014**, *6*, 188−195.
(11) Buzan, J. M.; Frieden, C. Yeast actin: Polymerization kinetic studies of wild type and a poorly polymerizing mutant. *Proc. Natl. Acad. Sci. U.S.A.* **1996**, *93*, 91−95.
(12) Vavylonis, D.; Yang, Q. B.; O'Shaughnessy, B. Actin polymerization kinetics, cap structure, and fluctuations. *Proc. Natl. Acad. Sci. U.S.A.* **2005**, *102*, 8543−8548.
(13) Frieden, C. Actin and Tubulin Polymerization - the Use of Kinetic Methods to Determine Mechanism. *Annu. Rev. Biophys.* **1985**, *14*, 189−210.
(14) Smulders, M. M. J.; Nieuwenhuizen, M. M. L.; de Greef, T. F. A.; van der Schoot, P.; Schenning, A. P. H. J.; Meijer, E. W. How to Distinguish Isodesmic from Cooperative Supramolecular Polymerisation. *Chem.—Eur. J.* **2010**, *16*, 362−367.
(15) Ley, D.; Guzman, C. X.; Adolfsson, K. H.; Scott, A. M.; Braunschweig, A. B. Cooperatively Assembling Donor-Acceptor Superstructures Direct Energy Into an Emergent Charge Separated State. *J. Am. Chem. Soc.* **2014**, *136*, 7809−7812.
(16) Gillissen, M. A. J.; Koenigs, M. M. E.; Spiering, J. J. H.; Vekemans, J. A. J. M.; Palmans, A. R. A.; Voets, I. K.; Meijer, E. W. Triple Helix Formation in Amphiphilic Discotics: Demystifying Solvent Effects in Supramolecular Self-Assembly. *J. Am. Chem. Soc.* **2014**, *136*, 336−343.
(17) Fennel, F.; Wolter, S.; Xie, Z. Q.; Plotz, P. A.; Kuhn, O.; Würthner, F.; Lochbrunner, S. Biphasic Self-Assembly Pathways and Size-Dependent Photophysical Properties of Perylene Bisimide Dye Aggregates. *J. Am. Chem. Soc.* **2013**, *135*, 18722−18725.
(18) Krieg, E.; Weissman, H.; Shimoni, E.; Bar On (Ustinov), A.; Rybtchinski, B. Understanding the Effect of Fluorocarbons in Aqueous Supramolecular Polymerization: Ultrastrong Noncovalent Binding and Cooperativity. *J. Am. Chem. Soc.* **2014**, *136*, 9443−9452.
(19) Serpe, M. J.; Craig, S. L. Physical organic chemistry of supramolecular polymers. *Langmuir* **2007**, *23*, 1626−1634.
(20) Korevaar, P. A.; Grenier, C.; Markvoort, A. J.; Schenning, A. P. H. J.; de Greef, T. F. A.; Meijer, E. W. Model-driven optimization of multicomponent self-assembly processes. *Proc. Natl. Acad. Sci. U.S.A.* **2013**, *110*, 17205−17210.
(21) Baram, J.; Weissman, H.; Tidhar, Y.; Pinkas, I.; Rybtchinski, B. Hydrophobic Self-Assembly Affords Robust Noncovalent Polymer Isomers. *Angew. Chem., Int. Ed.* **2014**, *53*, 4123−4126.
(22) Tidhar, Y.; Weissman, H.; Wolf, S. G.; Gulino, A.; Rybtchinski, B. Pathway-Dependent Self-Assembly of Perylene Diimide/Peptide Conjugates in Aqueous Medium. *Chem.—Eur. J.* **2011**, *17*, 6068−6075.
(23) Jiang, S. F.; ter Horst, J. H. Crystal Nucleation Rates from Probability Distributions of Induction Times. *Cryst. Growth Des.* **2011**, *11*, 256−261.
(24) Avrami, M. Kinetics of Phase Change. I General Theory. *J. Chem. Phys.* **1939**, *7*, 1103−1112.
(25) Christian, J. W.: *The theory of transformations in metals and alloys*; 1st ed.; Pergamon Press: Oxford, U.K., 1965.
(26) Yang, C. P.; Nagle, J. F. Phase transformations in lipids follow classical kinetics with small fractional dimensionalities. *Phys. Rev. A* **1988**, *37*, 3993−4000.
(27) Huang, T.; Tsuji, T.; Kamal, M. R.; Rey, A. D. Domain-spatial correlation functions and scaling relations of nucleation and growth in polymer films. *Phys. Rev. E* **1998**, *58*, 789−792.
(28) Herrick, J.; Jun, S.; Bechhoefer, J.; Bensimon, A. Kinetic model of DNA replication in eukaryotic organisms. *J. Mol. Biol.* **2002**, *320*, 741−750.
(29) Jun, S.; Zhang, H.; Bechhoefer, J. Nucleation and growth in one dimension. I. The generalized Kolmogorov-Johnson-Mehl-Avrami model. *Phys. Rev. E* **2005**, *71*, 011908.
(30) Chandler, D. Interfaces and the driving force of hydrophobic assembly. *Nature* **2005**, *437*, 640−647.
(31) Kotting, C.; Kallenbach, A.; Suveyzclis, Y.; Wittinghofer, A.; Gerwert, K. The GAP arginine finger movement into the catalytic site of Ras increases the activation entropy. *Proc. Natl. Acad. Sci. U.S.A.* **2008**, *105*, 6260−6265.
(32) Wilson, D. H.; Benight, A. S. Kinetic-Analysis of the Preequilibrium Steps in the Self-Assembly of Reca Protein from Escherichia-Coli. *J. Biol. Chem.* **1990**, *265*, 7351−7359.
(33) Rybtchinski, B.; Sinks, L. E.; Wasielewski, M. R. Combining Light-Harvesting and Charge Separation in a Self-Assembled Artificial Photosynthetic System Based on Perylenediimide Chromophores. *J. Am. Chem. Soc.* **2004**, *126*, 12268−12269.